Discovery of potent pteridine reductase inhibitors to guide antiparasite drug development

Antonio Cavazzuti*, Giuseppe Paglietti†, William N. Hunter‡, Francisco Gamarro§, Sandra Piras†, Mario Loriga†, Sergio Alleca†, Paola Corona†, Karen McLuskey‡, Lindsay Tulloch‡, Federica Gibellini*‡, Stefania Ferrari*, and Maria Paola Costi*¶

*Dipartimento di Scienze Farmaceutiche, Università di Modena e Reggio Emilia, Via Campi 183, 41100 Modena, Italy; †Dipartimento Farmaco Chimico Tossicologico, Università degli Studi di Sassari, via Muroni 23/a 07100 Sassari, Italy; ‡Division of Biological Chemistry and Drug Discovery, College of Life Sciences, University of Dundee, Dundee, DD1 5EH, United Kingdom; and §Instituto de Parasitologia y Biomedicina ''Lopez-Neyra,'' Consejo Superior de Investigaciones Cientificas, Parque Tecnológico de Ciencias de la Salud, Avenida del Conocimiento s.n., 18100 Armilla, Granada, Spain

Edited by Robert M. Stroud, University of California, San Francisco, CA, and approved November 26, 2007 (received for review May 10, 2007)

Pteridine reductase (PTR1) is essential for salvage of pterins by parasitic trypanosomatids and is a target for the development of improved therapies. To identify inhibitors of *Leishmania major* and *Trypanosoma cruzi* PTR1, we combined a rapid-screening strategy using a folate-based library with structure-based design. Assays were carried out against folate-dependent enzymes including PTR1, dihydrofolate reductase (DHFR), and thymidylate synthase. Affinity profiling determined selectivity and specificity of a series of quinoxaline and 2,4-diaminopteridine derivatives, and nine compounds showed greater activity against parasite enzymes compared with human enzymes. Compound 6a displayed a K_i of 100 nM toward *Lm*PTR1, and the crystal structure of the *Lm*PTR1:NADPH:6a ternary complex revealed a substrate-like binding mode distinct from that previously observed for similar compounds. A second round of design, synthesis, and assay produced a compound (6b) with a significantly improved K_i (37 nM) against *Lm*PTR1, and the structure of this complex was also determined. Biological evaluation of selected inhibitors was performed against the extracellular forms of *T. cruzi* and *L. major*, both wild-type and overexpressing PTR1 lines, as a model for PTR1-driven antifolate drug resistance and the intracellular form of *T. cruzi.* An additive profile was observed when PTR1 inhibitors were used in combination with known DHFR inhibitors, and a reduction in toxicity of treatment was observed with respect to administration of a DHFR inhibitor alone. The successful combination of antifolates targeting two enzymes indicates high potential for such an approach in the development of previously undescribed antiparasitic drugs.

antitrypanosomatid agents | antifolates | drug discovery

Protozoan parasites of the order Kinetoplastida are the causal agents of serious human diseases, including African sleeping sickness, Chagas' disease, and leishmaniasis. There is an urgent need for new, more effective drugs targeting these neglected diseases, because those in current use are toxic, expensive, and often difficult to administer. The problem is compounded by an increase in drug resistance and lack of progress in drug development. Only a single new effective treatment has been developed in the last 25 years, Miltefosine (hexadecylphosphocholine), recently approved in India (1).

Enzymes involved in the provision and use of reduced folate cofactors such as dihydrofolate reductase (DHFR) and thymidylate synthase (TS) are valued drug targets for the treatment of bacterial infections (2), cancer (3), and certain parasitic diseases, notably malaria (4). DHFR catalyzes the two-step reduction of folate to tetrahydrofolate, which is then transformed to N^5,N^{10}-methylene tetrahydrofolate and is used by TS as a methyl donor and reducing agent in the conversion of 2′-deoxyuridine-5′-monophosphate to 2′-deoxythymidine-5′-monophosphate. Inhibition of DHFR or TS reduces the cellular pool of 2′-deoxythymidine-5′-monophosphate, impairing DNA replication and resulting in cell death.

Because trypanosomatids are auxotrophic for folates and pterins, the inhibition of the enzymes depending on them should provide suitable treatments. However, antifolates are not used in the therapy of trypanosomatid infections mainly because of pteridine reductase (PTR1). Although the bifunctional DHFR-TS used by trypanosomatids can exclusively reduce folic acid, the short-chain dehydrogenase/reductase PTR1 shows a much broader range of activity catalyzing successive reductions of conjugated (folate) and unconjugated (biopterin) pterins (5, 6). Under physiological conditions, PTR1 is responsible of reduction of ≈10% of the folic acid required by the cell (7), but when classical antifolate drugs inhibit DHFR-TS, PTR1 can be overexpressed, allowing for significant reduction of the necessary amounts of folates to ensure parasite survival (8). This compensatory mechanism suggests that treatment of trypanosomatid infections could be achieved through inhibition of both DHFR and PTR1 by a single drug or a combination of molecules that are specific inhibitors of the two targets (7). A series of diaminopteridines and quinazolines have been tested against these enzymes and parasites, leading to identification of inhibitors with micromolar K_i (inhibition constant) values (9). Structures of PTR1 complexes with substrates, products, and inhibitors have illuminated aspects of ligand recognition and enzyme mechanism (10–12). Based on these data and with the intention of identifying potent inhibitors of *Leishmania major* and *Trypanosoma cruzi* enzymes, we analyzed a library of 440 synthetic folate-like compounds. Approximately one-third of these were selected for rapid screening against a panel of folate-dependent enzymes. The molecular interactions between two of the most potent inhibitors with PTR1 were elucidated by x-ray crystallography. The compounds that displayed the best inhibition profiles *in vitro* were subjected to biological evaluation on the protozoan parasites *L. major* and *T. cruzi* WT and overexpressing PTR1 lines, as well as on the intracellular form of *T. cruzi*. When the molecules were tested in combination with known DHFR inhibitors, additive profiles of inhibition were observed.

Results and Discussion

Our study considered a collection of 440 folate-related compounds originally designed as potential anticancer agents (13–15). Of these, 72 were recently synthesized to enrich the library. Compounds were evaluated on the basis of molecular diversity, lipophilicity, the

Author contributions: M.P.C. and S.F. designed research; and G.P., S.P., M.L., S.A., P.C., W.N.H., K.M., L.T., F. Gibellini, F. Gamarro, and A.C. performed research.

The authors declare no conflict of interest.

This article is a PNAS Direct Submission.

Data deposition: The atomic coordinates and structure factors have been deposited in the Protein Data Bank, www.pdb.org (PDB ID codes 2P8K and 2QHX).

¶To whom correspondence should be addressed. E-mail: mariapaola.costi@unimore.it.

This article contains supporting information online at www.pnas.org/cgi/content/full/0704384105/DC1.

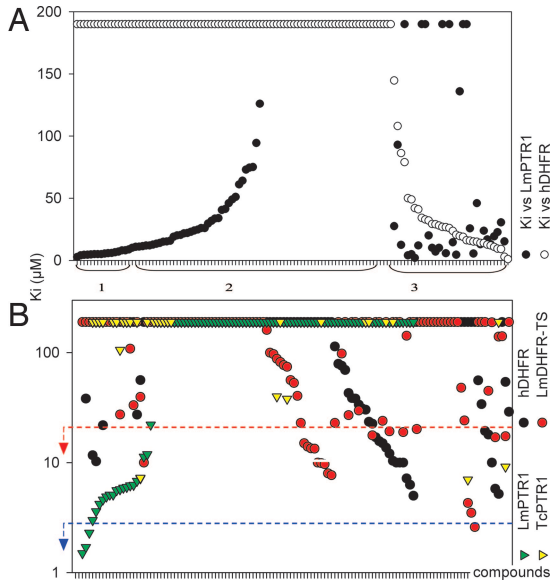

Fig. 1. Inhibition activity profiles of the 131 selected compounds. (*A*) Distribution profile of compounds toward human DHFR (white dot) and *Lm*PTR1 (solid black dots). It is possible to distinguish a first set of compounds with high specificity for *Lm*PTR1 (region 1), characterized by low-micromolar K_i on *Lm*PTR1 and lack of inhibition on human DHFR, followed by a series of compounds with no activity on both enzymes (region 2) and finally compounds inhibiting both enzymes (region 3). (*B*) Enzyme inhibition profiles (K_i). Logarithmic representation of K_i obtained in *in vitro* assay of enzyme inhibition for *h*DHFR (black), *Lm*DHFR-TS (red), *Lm*PTR1 (green), and *Tc*PTR1 (yellow). Cutoff lines for inhibitors with $K_i < 30$ μM (red) and $K_i < 3$ μM inhibitors (blue) are shown. Spots aligned at the top of the graph show no inhibition at 190 μM.

conformity to Lipinsky rules (16) and the presence of ionizable functional groups [following integrated Ferguson's principle (17)]. Previously reported toxicity data were considered and those compounds showing no cell-based anticancer activity preferred. The 131 molecules that fit the selection criteria were advanced to a rapid screening assay evaluation against a panel of folate-dependent enzymes, including TS from pathogenic and nonpathogenic species, *L. major* DHFR-TS, and *L. major* and *T. cruzi* PTR1. Inhibition of human TS and DHFR was used to estimate the toxicity/specificity of the compounds, and three biological profiles were observed: (*i*) no activity against both human enzymes at 190 μM (48% of compounds); (*ii*) inhibition of only one human enzyme (45%); and (*iii*) inhibition of both human enzymes (7%) (data not shown). Compounds that showed a specificity index (K_i human enzyme/K_i target enzyme) $\geq$100 with respect to at least one human enzyme (DHFR or TS) were considered suitable as antiparasitic leads. The inhibition profiles identified groups of compounds with strong specificity for *Lm*PTR1, with a lack of activity against *Lm*PTR1 and *h*DHFR or relevant activity with lack of specificity (Fig. 1*A*, regions 1, 2, and 3, respectively). This trend reflects a significant level of molecular diversity within the library and offers useful tools for structure–activity relationship analysis. A first selection was performed based on solubility in water and calculated $K_i \leq 30$ μM (at least 30% of inhibition at 190 μM). (Fig. 1*B*, red dashed line). Compounds that inhibited the enzymes with K_i values <3 μM (Fig. 1*B*, blue dashed line), corresponding to 70% inhibition at 20 μM inhibitor concentration, were selected for testing against the protozoan parasites *L. major* and *T. cruzi.* Finally, we selected representatives of all main chemical classes present in the original library: 2,4 diaminopteridines and quinoxalines with substituents in positions 2 and 6 (Table 1). K_i-based selection led to a reduction from 131 to 9 compounds (Table 1, first round). These nine compounds displayed a specificity index >100 against at least one human enzyme or showed an interesting enzyme profile and structure. Notably, compound **6a**, with a K_i of 7 μM against *Tc*PTR1 of 100 nM toward *Lm*PTR1 and of 4 μM against *Lm*DHFR, was the best inhibitor of *Lm*PTR1 and one of the most selective compounds in the series, with no detectable inhibition of *h*TS and a specificity index of equal or >100 toward *h*DHFR. Compounds **10n** and **9m** inhibited *Lm*PTR1 with K_i values of 7 and 6 μM, respectively, and 8-fold lower ratio of affinity/no affinity toward *h*DHFR. Compounds **65**, **66**, and **55** were moderately good inhibitors of *Lm*DHFR and showed no affinity toward *h*DHFR. The 2,4-diaminopteridine derivatives are similar to the natural substrates/cofactors for DHFR-TS and PTR1, and in general were not strong inhibitors of these enzymes with the notable exception of **6a**. However, the quinoxaline scaffold displayed an interesting profile of inhibition, suggesting an alternative approach to antifolate candidates with high substrate selectivity.

After the identification of compound **6a** as a potent and selective inhibitor of the parasite enzymes and having determined the crystal structure in complex with cofactor and *Lm*PTR1 (see below), the compound library was reevaluated to identify similar compounds for further testing (Table 1, second round). The selected compounds present a classical folate core structure with pteridinic or quinoxalinic head groups linked through the carboxylic group to different terminal groups (pyrrolidinic, piperidinic or glutamic groups). Compounds **6b**, **6c**, **59**, and **60** were tested against *Lm*PTR1 and the best inhibitors also against *h*DHFR. **6b** displayed K_i values of 37 and 820 nM against *Lm*PTR1 and *h*DHFR, respectively (Table 1). The other compounds showed little or no inhibition of *Lm*PTR1. Notably, compound **6c** is at least 3 orders of magnitude less active than compound **6a**, even though the only differences between them reside in the terminal portion of the glutamate tail (a piperidine moiety in **6a** vs. a pyrrolidine moiety in **6c**). Thus, even if the portion of the enzyme active site accommodating the terminus of the inhibitor is wide and disordered (due to the presence of flexible loops, as indicated in the x-ray structure), this part of the inhibitor can still influence the binding affinity of the molecule, possibly by steric hindrance and/or solvation effects.

Structures of LmPTR1–NADPH Inhibitor Complexes. Crystal structures of the ternary complex of enzyme, reduced cofactor, and the inhibitors **6a** and **6b** were determined at 2.4- and 2.6-Å resolution, respectively. The PTR1 subunit is a seven-stranded parallel β-sheet with three α-helices on either side. The active site is an elongated cleft $\approx$22 by 15 Å, created by the C-terminal sections of several of the β-strands, two α-helices, and an extended loop region (10). The cofactor binds in an extended conformation with the nicotinamide, creating the floor of the catalytic center, with Phe-113 forming an overhang under which the pterin-binding pocket is formed. Nearby are three important residues (Fig. 2). Tyr-194 is the active-site base, which acts in concert with Asp-181 to acquire and pass on one reducing equivalent. Lys-198 positions the nicotinamide through hydrogen-bonding interactions with the cofactor ribose and may reduce the pK_a of Tyr-194, thereby assisting catalysis (10, 12). The *Lm*PTR1-**6a** complex structure contains two tetramers, subunits labeled A-H, in the asymmetric unit. In each active site, the inhibitor adopts an orientation similar to that observed for substrate with the C7-N8 bond near Asp-181 and Tyr-194. The inhibitor forms hydrogen bonds with Ser-111, Tyr-194, the phosphate and ribose components of the cofactor, and an ordered water molecule (Fig. 2*A*). The asymmetric unit of the *Lm*PTR1-**6b** complex structure contains a tetramer, subunits labeled A-D, and the inhibitor displays two modes of binding (Fig. 2*B*). All four subunits of the asymmetric unit position the inhibitor in a methotrexate (MTX)-like binding mode, with the C7-N8 bond directed outward from the active site (Fig. 2*B*). The occupancy of **6b** in the MTX orientation in subunits C and D is 100%; however, in subunits A and B, the occupancy is 50:50 between the MTX orientation and a substrate-

Table 1. Inhibition constants (K_i, μM) of compounds selected for further biological evaluation on parasites

Name	Structure	TS		DHFR		PTR1	
		*h*TS	L*m*TS	*h*DHFR	L*m*DHFR	*Lm*PTR1	*Tc*PTR1
a-First-round screening							
6a	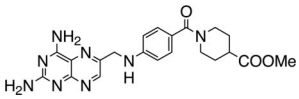	NI	NI	10	4	0.1	7
10n	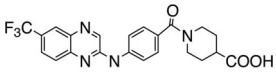	41	NI	56	40	7	75
10l	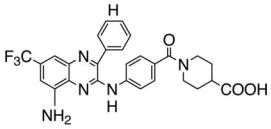	13	NI	54	17	—	20
9t	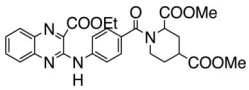	15	NI	24	75	NI	38
9j	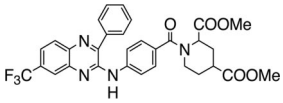	13	NI	NI	88	NI	40
9m	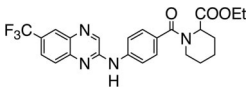	12	86	NI	27	6	106
65	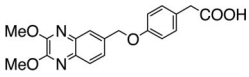	NI	NI	NI	3	—	—
66	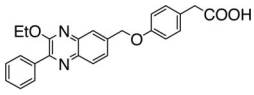	41	NI	NI	4	—	—
55	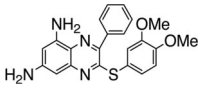	3	NI	NI	10	NI	NI
b-Second-round screening							
6b	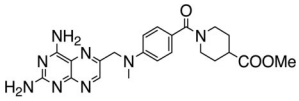	—	NI	0.8	—	0.037	—
6c	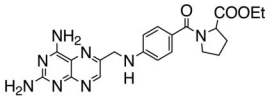	—	—	—	—	30%*	—
59	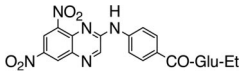	—	—	—	—	NI*	—
60	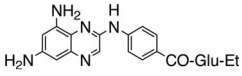	—	—	—	—	NI*	—
MTX	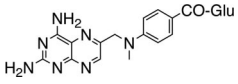	—	0.6	3.4†	130‡	0.18	0.11

NI, no inhibition at 190 μM; —, not tested.
*Tested at maximum concentration of 75 μM.
†K_i expressed in picomolar (39).
‡K_i expressed in picomolar (8).

like orientation. Our observation is consistent with a previous report that an MTX-type antifolate can adopt a nonclassical orientation in the DHFR active site (18).

In the substrate-like conformation (Fig. 2*B*), the head group of **6b** is sandwiched between the nicotinamide and Phe-113 with N1, N2, N3, and N4 atoms interacting with the cofactor. N1 and N2 form hydrogen bonds with the ribose 2′ OH, whereas N3 interacts with a cofactor phosphate. N2 interacts with the side and main chains of Ser-111, whereas N4 is separated from the Arg-17-NH_2 by a distance of 3.3 Å. In subunit B, the terminal portion ranging from the pterin head to the piperidine ring can be more precisely assigned to one conformation, with the N10

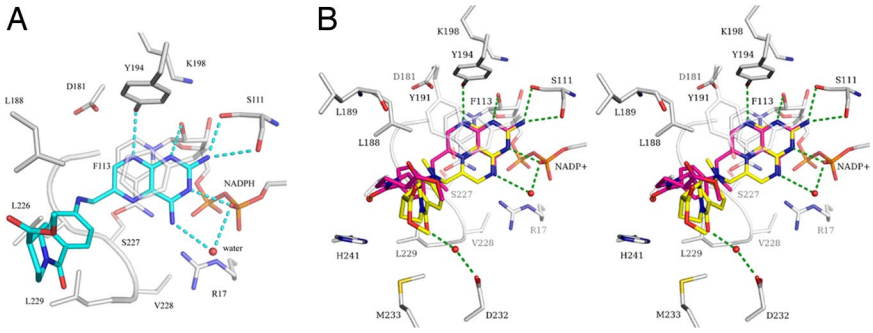

Fig. 2. PTR1 inhibition. (*A*) Compound **6a** adopts the substrate-like orientation. (*B*) Stereoview of the two orientations adopted by compound **6b** in subunit B of the ternary complex. C atoms of LmPTR1 and NADPH are gray, all O atoms are red, N atoms are blue, and the S atom of Met-233 is yellow. Two water molecules are shown as red spheres. Green dashed lines identify potential hydrogen bond interactions; Phe-113 and Tyr-191 are ghosted for clarity. The C atoms of the inhibitor that binds in the substrate-like orientation are purple and yellow for the inhibitor when it adopts the MTX-type orientation.

methyl oriented toward a hydrophobic site formed by Leu-226 and -229.

An overlay of the two binding modes displayed by **6b** is shown in Fig. 2*B*. A significant feature is that the catalytic Tyr-194 donates a hydrogen bond to the inhibitor when it adopts the substrate-like orientation but accepts a hydrogen bond donated from **6b** in the MTX-like orientation. That we observe two orientations for similar (**6a**, MTX) inhibitors or indeed the same molecule (**6b**) suggests little difference in the energy of binding. For **6a**, the steric freedom that arises because of lack of an N10 methyl substituent may tilt the balance toward the substrate-like orientation. For **6b**, the lack of interaction between the enzyme and the tail of the compound suggests that hydrogen-bonding capacity, which principally resides in the pteridine head group, is an important determinant of orientation. The hydrogen-bonding capacity offered by the active-site residues can be satisfied by two orientations, and that is what is observed. There may also be a solvent effect, because the N10 methyl group in one orientation, the MTX mode, is placed to disrupt a well ordered water network observed in that region of the active site (11, 12).

The differences between MTX or similar ligands binding to *h*DHFR and *Lm*PTR1 are striking [supporting information (SI) *Appendix*, SI Figs. 7 and 8] (10, 11). MTX, **6a**, and **6b** bind the PTR1:NADP$^+$ complex with the pteridine head group forming extensive interactions with the cofactor and the tail placed at the periphery of the active site with few interactions observed between ligand and enzyme. When MTX binds to *h*DHFR (19), there are few interactions (van der Waals) with the cofactor, all confined to the nicotinamide. The pteridine group and in particular the tail of MTX, however, form extensive electrostatic and van der Waals interactions with protein residues (*SI Appendix*, SI Fig. 8).

On-Parasite Assays. Growth inhibition assays were conducted on WT lines of epimastigote *T. cruzi* and promastigote *L. major* to test compound cytotoxicity. Dose–effect curves were obtained for all compounds and different profiles observed. Based on the EC_{50} values, only a few of the candidates were able to completely inhibit growth of parasites, with effects ranging from 40% of *T. cruzi* growth inhibition for **9j** to 100% of *L. major* growth inhibition for **9m** (data not shown). These results indicate that processes critical for parasite viability were targeted by the inhibitors. The implications of *ptr1* gene knockout on parasite viability are published (20); here, we evaluated the contribution of PTR1 in the mechanism of action of inhibitors by testing against parasite lines overexpressing this enzyme. A relative drug resistance (RDR) value, calculated by dividing EC_{50} obtained from the PTR1-overexpressing lines by the EC_{50} value obtained from WT lines (Fig. 3, EC_{50} in columns and RDR in line), was assessed by using as controls both WT parasites and parasites transfected with the empty vector (pTEX for *T. cruzi* and pX for *L. major*). The difference in biological activity (induced resistance) between the controls and overexpressing lines was assumed to be due to the different expression levels of PTR1. Classical DHFR inhibitors, such as MTX, pyrimethamine (PYR), aminopterin (AMP), and trimethoprim (TMP), were assayed for comparison, and two trends of biological activity were evident; compounds with RDR equal to 1 and those with RDR >1 (Fig. 3). An RDR >1 (**6a**, AMP, MTX in *T. cruzi* and **6a**, and **6b** in *L. major*) indicates that PTR1 inhibition is implicated in antiparasite activity. For compounds displaying an RDR value near 1 (**9m**, **9t** for *T. cruzi*), the growth inhibition of parasites is unrelated to PTR1 expression level, and the inhibitor likely has an alternative molecular target in both WT and overexpressing parasites. These results with **9m** and **9t** for *T. cruzi* epimastigote forms suggest that alternative, potentially valuable targets besides PTR1 and DHFR-TS exist.

Additionally, we have assayed the activity of selected compounds **6a** and **6b** on amastigote intracellular forms of *T. cruzi*. Both compounds were able to inhibit proliferation of amastigote *T. cruzi* demonstrating their ability to cross the plasma membrane of mammalian host Vero cells displaying their activity intracellularly. The effect of compounds **6a** and **6b** on amastigote growth inhibition was, respectively, 22% and 27% at 50 μM (*SI Appendix*, SI Fig. 12).

Synergy Evaluation. Selected compounds were combined with known DHFR inhibitors to test effects of coadministration on *T. cruzi* and *L. major* WT parasite lines. For each compound tested, at least one known inhibitor produced an additive inhibition, which permits a decrease in concentration of known DHFR-TS inhibitors,

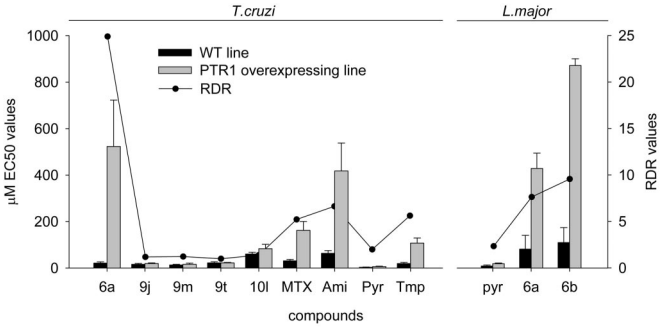

Fig. 3. EC_{50} and RDR values for *T. cruzi* (*Left*) and *L. major* (*Right*). Growth inhibition effect (μM EC_{50}, left *y* axis) induced by main compounds singularly administrated on WT (black bars) and PTR1 overexpressing lines (gray bars). RDR values obtained dividing EC_{50} from PTR1-overexpressing line by EC_{50} obtained from WT lines for each pair of data are plotted with black pointed line (values in right *y* axis).

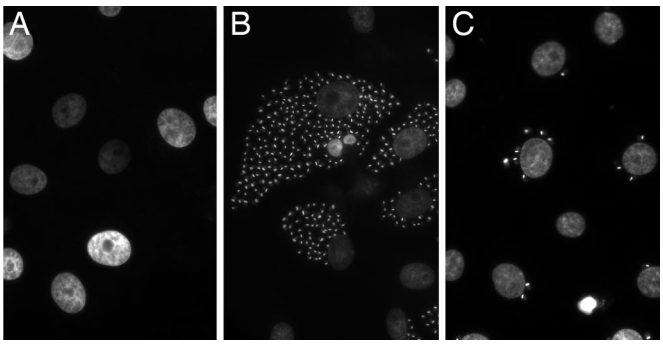

Fig. 4. Images obtained by fluorescence microscopy of samples stained with DAPI (2-(4-amidinophenyl)-6-indolecarbamidine) for evaluation of mean number of parasites per infected not treated (*B*) and treated (*C*) cells, compared with noninfected Vero cells (*A*). The nuclei of 9–10 Vero cells are visible in each camp. In *B* is shown as intracellular parasites (visualized as a small spot given by fluorescence of amastigote kinetoplast and nucleus) distributed in a monolayer when the adherent cell is not confluent with space to expand, facilitating their counting. When parasitism is high, the shape of the infected area corresponds to an area covered by the adherent cell. It is evident that in *C*, parasites that entered during the infection phase, before drug administration were not able to proliferate as in *B*.

characterized by a low therapeutic index, necessary to reach maximum effect. The importance of this observation resides in the low toxicity of the selected compounds (*SI Appendix*, SI Table 5). PYR was generally the best partner for inhibition of *T. cruzi*, where almost all associations produced additive inhibition, and *L. major* (SI Fig. 20). In the latter case, PYR was the only commercial inhibitor showing an additive effect with all selected hits. MTX, TMP, and AMP showed antagonist profiles against most of the tested compounds. Compounds **65** and **66,** in contrast, showed additive inhibition effects. Some combinations gave inhibition profiles that exceeded the expected value of 50%, as explained in *Materials and Methods.* Compound **66** with PYR gave an inhibition value of 63% against *L. major*, whereas **101** with PYR exhibited greater than expected growth inhibition (60%) against *T. cruzi*. *T. cruzi* displayed smaller differences in growth inhibition values than did *L. major* when the mentioned compounds were combined with known inhibitors (*SI Appendix*, SI Fig. 20). This differential effect may be related to the presence of additional targets (5, 21) specific to *T. cruzi* that could increase the growth inhibition caused by nonspecific DHFR inhibition.

The result of the combination of each selected compound **6a** and **6b** at 50 μM with PYR at 10 μM (the latter producing 66% amastigote growth inhibition when administered alone at that concentration) on intracellular amastigote forms of *T. cruzi* was additive, showing an amastigote growth inhibition of 83–88% when both compounds were mixed at the above concentrations (*SI Appendix*, SI Fig. 12). Compounds **6a** and **6b** showed a lower toxicity on mammalian cells (EC_{50} values of 580 and 331 μM, respectively) with respect to PYR (EC_{50} 22 μM). Consequently, the coadministration of compound **6a** (50 μM) with PYR (10 μM) efficiently reduced the toxicity of the treatment necessary to obtain 85% amastigote growth inhibition with a significantly reduced effect on Vero cells (25% of Vero cell death vs. 39% of Vero cell death by PYR required concentration to reach the same 85% amastigote growth inhibition).

Concluding Remarks. The screening of a folate-analogue library identified a potent selective inhibitor of *Lm*PTR1, named compound **6a**. Crystallographic analysis revealed **6a** interacting with the enzyme with a binding mode in which the pteridine is rotated by 180° with respect to the pteridine of MTX. Based on this finding, additional compounds were retrieved from the library, seeking to investigate the structural features responsible for this altered binding mode and to improve binding affinity. Compound **6b**, with an N10 methyl substituent, is well suited to the purpose of understanding the involvement of this group in the establishment of a particular binding mode. The crystal structure of *Lm*PTR1-NADPH-**6b** suggested that **6b** is able to satisfy the hydrogen binding capacity offered by the active site, and the cost of disruption of a water network might explain the different orientations observed. The database of folate analogues was reexamined to identify compounds showing similarity with **6a** and inhibition constants determined. The best PTR1 inhibitors were tested against WT and engineered *L. major* and *T. cruzi* parasites overexpressing PTR1, but these compounds showed poor efficacy when tested singly. However, when used in combination with known DHFR inhibitors, especially PYR, an additive profile was observed to be deleterious to parasite cell growth. The same behavior was observed when using the intracellular amastigote forms of *T. cruzi*, with the advantage of a reduced toxicity of treatment because of lower concentrations of DHFR-TS targeting drug. This work describes a successful combination of two antifolates designed to target DHFR-TS and PTR1. The challenge now is to exploit our understanding of this system to explore and develop a more potent combination that provides synergistic inhibition at a level that ultimately might provide an alternative therapeutic approach against this important class of pathogens.

Materials and Methods

Chemistry. The synthesis of 368 compounds in the library is published (e.g., refs. 22–24).

***Synthesis of compound* 6a**. To a solution of methyl 1-(4-aminobenzoyl)piperidine-4-carboxylate (compound **4a,** *SI Appendix, SI Text*) (100 mg, 0.36 mmol) in 3 ml of DMA was added an equimolar amount of 6-bromomethyl-2,4-diaminopteridine hydrobromide (compound **7,** *SI Text*), synthesized as referenced (23–25). The solution was stirred and kept at room temperature for 90 h. The solvent was removed by evaporation *in vacuo* (<1 mm Hg, bath to 45°C). The residue was purified by flash chromatography using $CHCl_3$/MeOH (9:1, vol/vol) as eluent to afford the **6a** as a solid (65 mg, 50% yield).

***Synthesis of compound* 6b**. To a solution of methyl 1-(4-methylaminobenzoyl)piperidine-4-carboxylate (compound **5**, *SI Appendix, SI Text*) (120 mg, 0.43 mmol) in 3 ml of DMA was added an equimolar amount of 6-bromomethyl-2,4-diaminopteridine hydrobromide (compound **7**, *SI Appendix, SI Text*), synthesized as reported (22–24). The solution was stirred and kept at room temperature for 84 h. The solvent was removed by evaporation *in vacuo* (<1 mm Hg, bath to 45°C). The residue was purified by flash chromatography using $CHCl_3$/MeOH (9:1, vol/vol) as eluent to afford **6b** as a solid (110 mg, 50% yield). Synthetic methods for the remaining 70 compounds together with selected analytical data are described in the *SI Appendix, SI Text*.

Analytical Methods. Melting points were recorded on a Köfler hot stage or Digital Electrothermal melting point apparatus and are uncorrected. Infrared spectra were recorded as nujol mulls on NaCl plates with a Perkin–Elmer 781 IR spectrophotometer and are expressed in ν (cm^{-1}). UV spectra are qualitative and were recorded in nanometers for solutions in EtOH with a Perkin—Elmer Lamba 5 spectrophotometer. NMR (^{1}H-NMR and NOE difference) spectra were determined in $CDCl_3$, DMSO-d_6, $CDCl_3$/DMSO-d_6 (in the ratio 1:3) with a Varian XL-200 (200 MHz). Chemical shifts (δ scale) are reported in parts per million downfield from tetramethylsilane as internal standard. Splitting patterns are designated as follows: s, singlet; d, doublet; t, triplet; q, quadruplet; m, multiplet; br s, broad singlet; and dd, double doublet.

The assignment of exchangeable protons (OH and NH) was confirmed by the addition of D_2O. Mass spectroscopy was performed on combined HP 5790–HP 5970 GC/MS apparatus or with a combined liquid chromatograph–Agilent 1100 series Mass Selective Detector (Agilent). Elemental analyses were performed on a Perkin–Elmer 2400 instrument, and the results for C, H, and N were within ± 0.4% of theoretical values.

Materials. Analytical TLC was performed on Merck silica gel F-254. For flash chromatography Merck silica gel 60 was used with a particle size 0.040–0.063 mm (230–400 mesh; Americal Society for Testing and Materials). Commercial reagents were used without further purification.

Selection of Inhibitors. Compounds were selected on the basis of a lack of antiproliferative activity toward human cell lines with reference to the National

Cancer Institute, Bethesda [National Cancer Institute (NCI)] studies for anticancer agents. The data were available following an *in vitro* disease-oriented antitumor screening program against a panel of 60 human tumor cells lines, in the NCI. The compounds showed an inhibitory potency <40% in a dose–response curve, in the NCI test that produced 50% growth inhibition, total growth inhibition, and 50% cytotoxicity data (12, 25).

The second criterion was molecular diversity. The database contained quinoxalines and 2,4-diaminopteridines. Simple molecular properties such as solubility, presence of a glutamate tail, salt, or free carboxylic acid functionality were also considered in selection. Finally, from >400 compounds, 131 were tested in rapid screening assays.

The molecules were tested against the following enzymes. Human TS and DHFR, *Escherichia coli* TS, *Lactobacillus casei* TS, *Enterococcus faecalis* TS, *L. major* DHFR-TS, *T. cruzi* DHFR-TS, *L. major* PTR1, *T. cruzi* PTR1. Raw IC_{50} values against the different enzymes, assuming competitive inhibition with respect to substrate, were obtained and K_i values calculated (26). For TS, the competitor substrate was N^5,N^{10}-methylenetetrahydrofolate; for DHFR, dihydrofolic acid, and for PTR1, folic acid. Data analysis was conducted and the first considerations were performed on the grouping of human and non-human enzyme inhibitors. Assays were carried out in triplicate, and no individual measurement differed by >20% from the mean.

Crystallographic Analyses. Crystallographic analyses followed established methods (11, 27) and are detailed in *SI Appendix* together with statistics (*SI Appendix*, SI Table 2) and examples of omit electron density maps (*SI Appendix*, SI Fig. 5).

Target Protein Expression and *in Vitro* Inhibition Assay of Purified Enzymes. Proteins were purified as described (28–36). For the determination of TS activity, the oxidation of cofactor N^5,N^{10}-methylentetrahydrofolic acid was followed spectrophotometrically at 340 nm (29, 30). For determination of reductase activity (*h*DHFR, *Lm*DHFR, *Tc*DHFR, *Lm*PTR1, and *Tc*PTR1), NADPH oxidation was followed at 340 nm (8). All kinetic studies were performed in continuous assays executed in a Beckman DU640 spectrophotometer (26). The activity assays for PTR1 inhibition studies were performed at 303 K in the presence of NADPH (usually 100 μM) and folic acid (30 μM) at pH 6.0 in sodium phosphate buffer. For this reaction, PTR1 was incubated with folic acid and the reaction initiated with NADPH. K_m was determined by measuring the enzyme activity dependence on substrate concentration using folic acid as a substrate. Average K_m was 8 μM for PTR1. The inhibition assays were performed by adding increasing concentrations of inhibitor solubilized in 100% DMSO. DMSO concentration was kept below the concentration affecting enzymes activity (1% for PTR1, 8% for TS).

Cell Culture. WT, WT- pX, and WT-pX-PTR1 (*SI Appendix, SI Text* and SI Fig. 9) promastigote forms of *L. major* (strain 260) were grown at 28°C in M-199 medium (Gibco) supplemented with 10% heat-inactivated FBS (hiFBS, Gibco). WT, WT-pTEX, and WT-pTEX-PTR1 (35) epimastigote forms of *T. cruzi* (CL-Brener *II* strain) strains were grown in liver infusion tryptose medium supplemented with 10% hiFBS at 28°C. The parasite cultures were initiated with 4×10^6 cells per ml^{-1} and collected in the exponential phase of parasite growth. Trypomastigote forms of *T. cruzi* were obtained according to the method described (37) by infection of Vero cells (American Type Culture Collection CRL-1586), maintained in RPMI medium 1640 (Gibco BRL) supplemented with 5% FBS at 37°C. Semiconfluent Vero cell cultures were infected with trypomastigotes to obtain both amastigote and trypomastigote forms of *T. cruzi*.

Parasite Growth Inhibition Studies. The inhibition profile of selected compounds on the WT and transfected protozoan parasites was assessed by culturing the cells in the presence of different concentrations of inhibitors. After 72 h of incubation at 28°C, the viability of parasites was determined by the colorimetric assay (MTT, [3-(4,5-dimethylthiazol-2-yl)-2,5-diphenyltetrazolium bromide]) (38, 39). For drug evaluation on the intracellular amastigote forms of *T. cruzi*, we used an experimental model of intracellular forms obtained after the infection of Vero cells, as host mammalian cells, with the infective trypomastigote metacyclic forms of *T. cruzi* (37). Infection was obtained by inoculation and *in vitro* culture of Vero cells with trypomastigote forms at a rate of 10 parasite per cell. After 4 h of infection, infected cell cultures were washed with PBS, and fresh culture media containing the selected inhibitors were added. After 72 h of culture, samples were fixed with *p*-formaldehyde 4% and stained with the nucleus-selective fluorescent marker DAPI (2-(4-amidinophenyl)-6-indolecarbamidine). Counting of intracellular amastigotes was performed by ''Analize Particles'' function in image processing software ImageJ 1.38x (http://rsb.info.nih.gov/ij) 1.38x on 10 random selected visual camps for sample analysis were evaluated and an average of 250 mammalian cells counted.

Synergy Evaluation. For combinatory-effect determination of selected inhibitors, extracellular parasites were exposed in separate wells to EC_{50} doses of commercial inhibitors and selected compounds, defined in previous cytotoxicity assays. Within the same 96-well plate, the viability of parasites was assessed concomitantly with isoeffective concentrations of selected compounds and commercial inhibitors (*SI Appendix*, SI Fig. 20). Using intracellular amastigotes of the protozoan parasite *T. cruzi*, we assessed the mean number of parasites per infected cell after treatment with inhibitors administered singularly. The sum of the independent percentage of amastigote growth inhibition was compared with the effect obtained by coadministration of inhibitors at the same concentrations (40, 41).

ACKNOWLEDGMENTS. This work was funded by Ministero Istruzioni Università Ricerca–Fondi di Investimento per la Ricerca di Base RBAU01S38Z (M.P.C.), the Wellcome Trust and Biotechnology and Biological Sciences Research Council (W.N.H.), Spanish Grant ISCIII-Red de Investigación Cooperativa en Enfermedades Tropicales (RICET) RD06/0021/0002 (to F. Gamarro), and the European Union Marie Curie Host Fellowships (QLK2-CT-2001-60091 (to F. Gibellini). We thank the European Synchrotron Radiation Facility for beam time, Charles Bond and Alexander Schüttelkopf for discussions, Eprova for providing substrates, and S. Beverley, Washington University, St. Louis, MO, for reagents.

1. Sundar S, Makharia A, More DK, Agrawal G, Voss A, Fischer C, Bachmann P, Murray HW (2000) *Clin Infect Dis* 31:1110–1113.
2. Then RL (2004) *J Chemother* 16:3–12.
3. McGuire JJ (2003) *Curr Pharmacol Des* 9:2593–2613.
4. Gregson A, Plowe CV (2005) *Pharmacol Rev* 57:117–145.
5. Senkovich O, Pal B, Schormann N, Chattopadhyay D (2003) *Mol Biochem Parasitol* 127:89–92.
6. Cunningham ML, Titus RG, Turco SJ, Beverley SM (2001) *Science* 292:285–287.
7. Nare B, Luba J, Hardy LW, Beverley S (1997) *Parasitology* 114 (Suppl):S101–S110.
8. Bello AR, Nare B, Freedman D, Hardy L, Beverley SM (1994) *Proc Natl Acad Sci USA* 91:11442–11446.
9. Hardy LW, Matthews W, Nare B, Beverley SM (1997) *Exp Parasitol* 87:157–169.
10. Gourley DG, Schüttelkopf AW, Leonard GA, Luba J, Hardy LW, Beverley SM, Hunter WN (2001) *Nat Struct Biol* 8:521–525.
11. Schüttelkopf AW, Hardy LW, Beverley SM, Hunter WN (2005) *J Mol Biol* 352:105–116.
12. Dawson A, Gibellini F, Sienkiewicz N, Tulloch LB, Fyfe PK, McLuskey K, Fairlamb AH, Hunter WN (2006) *Mol Microbiol* 61:1457–1468.
13. Piras S, Loriga M, Paglietti G (2004) *Farmaco* 59:185–194.
14. Corona P, Vitale G, Loriga M, Paglietti G, Costi MP (1998) *Farmaco* 53:480–493.
15. Costi MP, Ferrari S, Venturelli A, Calo S, Tondi D, Barlocco D (2005) *Curr Med Chem* 12:2241–2258.
16. Lipinski CA, Lombardo F, Dominy BW, Feeney PJ (2001) *Adv Drug Rev* 46:3–26.
17. Alberti CG, Villa L (1984) in *Chimica Farmaceutica*, (Organizzazione Editoriale Medico Farmaceutica, Milan, Italy), pp 265–270.
18. Gangjee A, Yu J, McGuire JJ, Cody V, Galitsky N, Kisliuk RL, Queener SF (2000) *J Med Chem* 43:3837–3851.
19. Cody V, Luft JR, Pangborn W (2005) *Acta Crystallogr D* 61:147–155.
20. El Fadili A, Kundig C, Roy G, Ouellette M (2004) *J Biol Chem* 279:18575–18582.
21. Schormann N, Pal B, Senkovich O, Carson M, Howard A, Smith C, Delucas L, Chattopadhyay D (2005) *J Struct Biol* 152:64–75.
22. Baugh CM, Shaw E (1964) *J Org Chem* 29:3610–3612.
23. Piper JR, Montgomery JA (1974) *J Het Chem* 11:279–280.
24. Piper JR, Montgomery JA (1977) *J Org Chem* 42:208–211.
25. Loriga M, Piras S, Paglietti G, Costi MP, Venturelli A (2003) *Farmaco* 58:51–61.
26. Segel IH (1975) *Enzyme Kinetics. Behaviour and Analysis of Rapid Equilibrium and Steady-State Enzyme Systems* (Wiley, New York).
27. McLuskey K, Gibellini F, Carvalho P, Avery MA, Hunter WN (2004) *Acta Crystallogr D* 60:1780–1785.
28. Dann JG, Ostler G, Bjur RA, King RW, Scudder P, Turner PC, Roberts GC, Burgen AS (1976) *Biochem J* 157:559–571.
29. Hanahan D (1983) *J Mol Biol* 166:557–580.
30. Meek TD, Garvey EP, Santi DV (1985) *Biochemistry* 24:678–686.
31. Maley GF, Maley F (1988) *J Biol Chem* 263:7620–7627.
32. Santi DV, Edman U, Minkin S, Greene PJ (1991) *Protein Expr Purif* 2:350–354.
33. Livi LL, Edman U, Schneider GP, Greene PJ, Santi DV (1994) *Gene* 150:221–226.
34. Pedersen Lane J, Maley GF, Chu E, Maley F (1997) *Protein Expr Purif* 10:256–262.
35. Robello C, Navarro P, Castanys S, Gamarro F (1997) *Mol Biochem Parasitol* 90:525–535.
36. Gourley DG, Luba J, Hardy LW, Beverley SM, Hunter WN (1999) *Acta Crystallogr D* 1608–1610.
37. Torres C, Pérez-Victoria FJ, Parodi A, Castanys S, Gamarro F (2004) *Mol Microbiol* 54:632–646.
38. Mosmann T (1983) *J Immunol Methods* 65:55–63.
39. Alfieri SC, Zilberfarb V, Rabinovitch M (1987) *Parasitology* 95:31–41.
40. Lambert RJ, Lambert R (2003) *J Appl Microbiol* 95:734–743.
41. Gessner PK (1995) *Toxicology* 105:161–179.